


## Altermagnetic Routes to Majorana Modes in Zero Net Magnetization

Sayed Ali Akbar Ghorashi<sup>1,\*</sup>, Taylor L. Hughes,<sup>2</sup> and Jennifer Cano<sup>1,3</sup>

<sup>1</sup>*Department of Physics and Astronomy, Stony Brook University, Stony Brook, New York 11794, USA*

<sup>2</sup>*Department of Physics and Institute for Condensed Matter Theory, University of Illinois at Urbana-Champaign, Illinois 61801, USA*

<sup>3</sup>*Center for Computational Quantum Physics, Flatiron Institute, New York, New York 10010, USA*

 (Received 16 June 2023; revised 20 May 2024; accepted 9 August 2024; published 5 September 2024)

We propose heterostructures that realize first and second order topological superconductivity with vanishing net magnetization by utilizing altermagnetism. Such platforms may offer a significant improvement over conventional platforms with uniform magnetization since the latter suppresses the superconducting gap. We first introduce a 1D semiconductor-superconductor structure in proximity to an altermagnet that realizes end Majorana zero modes (MZMs) with vanishing net magnetization. Additionally, a coexisting Zeeman term provides a tuning knob to distinguish topological and trivial zero modes. We then propose 2D altermagnetic platforms that can realize chiral Majorana fermions or higher order corner MZMs. Our Letter paves the way toward realizing Majorana boundary states with an alternative source of time-reversal breaking and zero net magnetization.

DOI: [10.1103/PhysRevLett.133.106601](https://doi.org/10.1103/PhysRevLett.133.106601)

Realizing a topological superconductor (TSC) has been a driving force in the development of topological phases of matter, motivated by producing Majorana states for quantum computation [1–4]. While intrinsic realizations remain elusive, much research has been devoted to engineering hybrid platforms that realize TSCs in 1D nanowires and 2D heterostructures [5–14].

The three main ingredients in these platforms are superconductivity, spin-orbit coupling, and a time-reversal breaking element (e.g., an applied magnetic field, an adjacent ferromagnet, or magnetic adatoms). However, despite intense efforts, a definitive realization of Majorana qubits is still lacking [15–18]. The main challenges are (i) the detrimental effect of disorder, which can create accidental states below the superconducting gap that are difficult to distinguish from protected Majorana zero modes (MZMs), and (ii) control of the proximity-induced superconducting gap, which is typically suppressed by the time-reversal breaking element.

In this Letter, we introduce a new platform to address both problems by realizing MZMs in a system with *vanishing net magnetization*, which allows further tunability with a Zeeman field that can distinguish disorder-induced subgap modes from topological MZMs. The new ingredient is altermagnetism. Altermagnets are a class of collinear antiferromagnets with a momentum-dependent magnetic order parameter [19,20] that have recently attracted attention [21–27], though they have been studied previously as Fermi surface instabilities [28]. Crucially, despite their vanishing magnetization, altermagnets can

generate sizable spin splitting, which changes sign in different regions of the Brillouin zone (BZ). For the sake of concreteness, we here focus on a *d*-wave magnetic order parameter, which describes the order of, e.g., RuO<sub>2</sub> [20]. However, the route we propose should generalize to order parameters with higher angular momenta.

We show that 1D and 2D TSCs hosting MZMs and chiral Majorana fermions (CMFs), respectively, can be realized in heterostructures where an altermagnet replaces the time-reversal breaking element. In addition to MZMs and CMFs, this platform can also realize higher order topological insulator (HOTI) and higher order TSC phases in two dimensions. Importantly, in one dimension a weak uniform magnetization or Zeeman field provides a knob to distinguish disorder-induced midgap states from protected MZMs.

*Majorana nanowire: MZMs without magnetic field*—We first consider a 1D semiconducting (SM) nanowire on the surface of an altermagnet and in proximity to an *s*-wave superconductor (SC), shown in Fig. 1(a). The Bogoliubov–de Gennes (BdG) Hamiltonian of the nanowire can be written as

$$h(k) = [\epsilon(k) + \lambda_R \sin(k)\sigma^2 + J_A \cos(k)\sigma^3] \tau^3 + \Delta \tau^2 \sigma^2, \quad (1)$$

where  $\epsilon(k) = t \cos(k) - \mu$ ,  $\tau$  and  $\sigma$  are Pauli matrices in Nambu and spin space, respectively,  $t$  is the hopping strength,  $\lambda_R$  is the strength of the Rashba spin-orbit coupling, and  $J_A$  and  $\Delta$  denote the proximity-induced altermagnetism and superconducting pairing, respectively. Importantly, the induced altermagnetism in the wire is specific to coupling to a  $d_{x^2-y^2}$ -wave altermagnet and depends sensitively on the orientation of the altermagnet:

\*Contact author: [sayedaliakbar.ghorashi@stonybrook.edu](mailto:sayedaliakbar.ghorashi@stonybrook.edu)

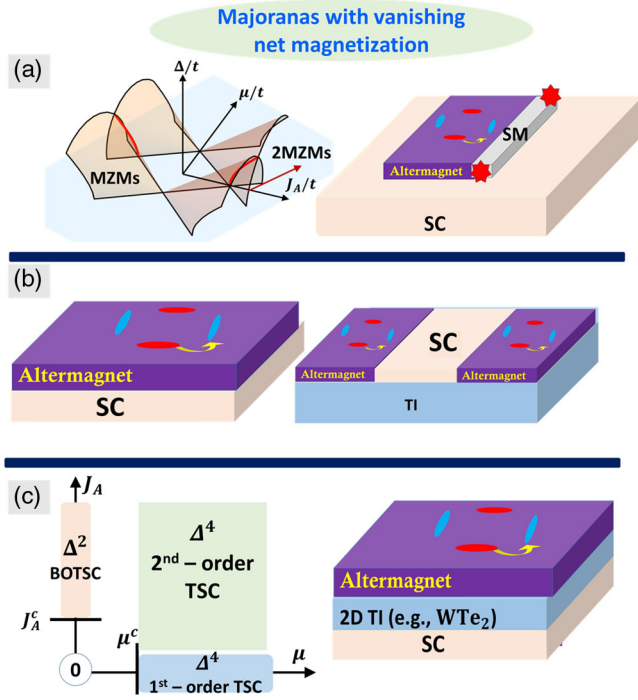


FIG. 1. Proposed setups using altermagnets to realize topological superconductivity with vanishing net magnetization. (a) A 1D altermagnet-semiconductor (SM)-superconductor (SC) wire hosts single (shaded area) and multiple (along  $\mu/t = 0$ ; red line shows the boundary) MZMs, also indicated by red stars on right. (b) 2D altermagnet-SC and altermagnet-SC-3D topological insulator (TI) heterostructures generate chiral Majorana modes. (c) An altermagnet-SC-2D TI heterostructure hosts corner MZMs.

a  $d_{xy}$ -wave altermagnet yields  $J_A = 0$ , incompatible with MZMs (see Appendix A [29]). This crystal anisotropy is intrinsic to altermagnets and can provide improved detection and characterization of MZMs. Later we will show a similar angular dependence in two dimensions. Therefore, introducing altermagnetism adds crystal anisotropy as a novel tuning knob for designing topological superconductors.

The Hamiltonian is in class BDI, which has a  $\mathbb{Z}$  classification; this effective Hamiltonian has more symmetry than the physical quasi-1D nanowire, which is in class D [30–33]. It is topologically nontrivial when  $\sqrt{\Delta^2 + (t - \mu)^2} < J_A < \sqrt{\Delta^2 + (t + \mu)^2}$ , where, despite vanishing net magnetization, a finite-sized wire hosts MZMs at its ends, shown in Fig. 2(a). Similar to the case of uniform magnetization, MZMs arise when the nanowire has an odd number of partially filled subbands gapped by the superconductivity. By eliminating the net magnetization, the altermagnetic heterostructure offers a significant improvement over uniform magnetization, which suppresses the superconducting gap [16,34]. Furthermore, ignoring this effect and assuming the same value of  $\Delta$  in Eq. (1), we show in Appendix B [29] that the topological gap in a heterostructure with an altermagnet generically

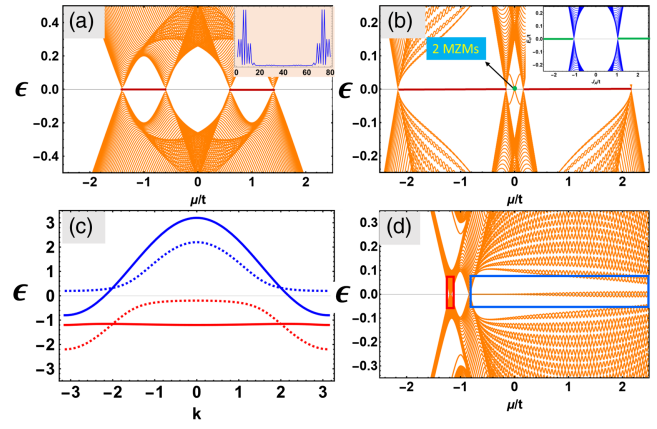


FIG. 2. Spectra of a nanowire heterostructure with vanishing net magnetization. (a) Finite-size spectrum of SC-proximitized nanowire vs  $\mu$  with  $\lambda_R = 0.5t$ ,  $J_A = 0.5t$ ,  $\Delta = 0.3t$ ; red lines show MZMs; inset shows the LDOS of MZMs. (b) Finite-size spectrum vs  $\mu$  ( $\mu = 0$ ) where green lines show two MZMs. (c) Bulk spectrum of nanowire with  $\lambda_R = 0.6t$ ,  $J_A = 1.2t$ ,  $J_Z = t$  (solid), and  $J_Z = 0$  (dashed) and (d) the corresponding finite-size spectra for solid lines in (c) vs  $\mu$  with  $\Delta = 0.1t$ . MZMs appear only when the chemical potential resides in the dispersive blue band in (c) [blue box in (d)].

exceeds that for uniform magnetization. Therefore, altermagnetism may provide a more robust topological phase compared to uniform magnetization. The effectiveness of the altermagnet in replacing the ferromagnet relies on it not vanishing on generic Fermi surfaces; this is the crux of designing TSCs with altermagnets, as will become more clear when we consider 2D models.

While our altermagnet can directly reproduce the MZMs seen in ferromagnetic systems, we also find phenomena that distinguish the two. One example is the dependence of the Zeeman term on the orientation of the wire, as mentioned below Eq. (1). Second, Fig. 2(b) shows the open boundary spectrum as a function of  $\mu$  for  $|J_A| > |t|$ ,  $\alpha = 0.5t$ ,  $\Delta = 0.3t$ . In this regime, the altermagnetism, combined with the Rashba term, generates a nontrivial Su-Schrieffer-Heeger [35] phase in the normal state, i.e., the two normal-state bands each have a  $\pi$  Berry phase. When  $\mu$  is in the insulating gap, the resulting superconducting phase will have a pair of MZM end states arising from the single complex fermion bound state in the normal state. Generically, these MZMs couple and open a gap. However, if  $\mu$  is tuned so that the edge modes in the normal state are at zero energy, which occurs at  $\mu = 0$  for the Hamiltonian in Eq. (1), then the resulting MZMs will be degenerate, as in Fig. 2(b). If  $|t| > |J_A|$ , there is generically an indirect gap closing for  $\mu \sim 0$  and no boundary MZMs. Note this physics does not occur in uniform magnetization, for which the normal phase is a trivial 1D insulator when magnetism is stronger than  $t$ .

Importantly, our model in Eq. (1) also has a useful sensitivity to an applied magnetic Zeeman field. Explicitly,

consider a weak external magnetic field, which induces a Zeeman term  $J_Z \hat{\mathbf{B}} \cdot \boldsymbol{\sigma}$  in the normal state. The application of a Zeeman field parallel to the altermagnet axis tunes the bandwidth of the subbands: Fig. 2(c) shows a generic regime where a Zeeman field parallel to the altermagnet axis can suppress the bandwidth and flatten one of the spin-split subbands. This should be contrasted with the ferromagnetic case where a Zeeman field perpendicular to the Rashba term will modify the spin-split subband gaps, but will not exhibit such bandwidth tuning. As a consequence of the band flattening, the open-boundary spectra in Fig. 2(d) exhibit a dramatic asymmetry as a function of  $\mu$ , displaying narrow and wide topological regions corresponding to gating into the narrow or wide subbands in Fig. 2(c). When  $\mu$  is in the narrow band, the presence of MZMs can be easily tuned using a weak Zeeman field. Since spurious subgap states created by nonmagnetic disorder will not be as sensitive to the applied field, this effect distinguishes nontopological and topological bound states. A Zeeman field perpendicular to the altermagnetic axis does not show a similar effect.

*Chiral Majorana fermions with zero net magnetization*—We now study 2D altermagnetic heterostructures shown in Fig. 1(b) that can host chiral modes and, in the presence of superconductivity, CMFs.

*Approach I: Altermagnet-3D TI interfaces*—3D time-reversal-invariant topological insulators (3D TIs) in proximity to a superconductor and time-reversal breaking magnetic element can exhibit CMFs [13,14,36]. We propose to replace the magnetic element with an altermagnet. The key requirement, as mentioned earlier, is that the topological surface states must reside at momenta where the altermagnetic order is nonvanishing and can open a gap.

We first discuss the normal phase. Consider depositing an altermagnet with order parameter  $(\cos k_x - \cos k_y)\sigma^3$  on the  $\hat{z}$ -normal surface of a 3DTI. In the case of perfect crystal alignment, the altermagnetism can open gaps of opposite sign on surface Dirac cones at the  $X = (\pi, 0)$  and  $Y = (0, \pi)$  points of the surface Brillouin zone, but leaves cones at  $\Gamma = (0, 0)$  and  $M = (\pi, \pi)$  gapless. (If the altermagnetism persisted in the bulk it could yield a 3D HOTI with chiral hinge modes [37,38].) Thus, for a 3D TI with a single Dirac cone at  $X$  or  $Y$ , there will be a single chiral mode at a domain wall where the altermagnetic order parameter changes sign. (Other configurations of altermagnetic domain walls hosting chiral modes are discussed in Appendix C [29]).

Now consider adding an  $s$ -wave SC: the chiral Dirac fermion at the domain wall will become a CMF. Similarly, a 3DTI with two altermagnets and an  $s$ -wave SC arranged laterally on one surface [Fig. 1(b), right] yields a chiral SC with CMFs along each SC-altermagnet boundary. We conclude that the ferromagnetic element can be replaced by an altermagnet as long as the 3DTI surface states reside at momenta off the nodal lines or surfaces of the altermagnet.

*Approach II: Bulk altermagnet or superconductor heterostructures*—We simplify the platform by removing the 3DTI and considering altermagnet-SC heterojunctions as in Fig. 1(b), left. We model an altermagnet layer coupled to a SC layer with  $s$ - and/or  $d$ -wave singlet pairing by the Hamiltonian:

$$H_I(\mathbf{k}) = [\epsilon(\mathbf{k}) - \mu]\tau^3 + \lambda_R(\mathbf{k}) + J_A(\mathbf{k}) + \Delta(\mathbf{k})\tau^2\sigma^2, \quad (2)$$

where  $\epsilon(\mathbf{k}) = t[\cos(k_x) + b_1 \cos(k_y)]$ ,  $\lambda_R(\mathbf{k}) = \lambda_R[\sin(k_x)\tau^3\sigma^2 - \sin(k_y)\tau^0\sigma^1]$ ,  $J_A(\mathbf{k}) = J_A[\cos(k_x) - b_2 \cos(k_y)]\tau^3\sigma^3$ ,  $\Delta(\mathbf{k}) = \Delta_0 + \Delta_1[\cos(k_x) + b_3 \cos(k_y)]$ ;  $t, \lambda_R, J_A, \Delta_{0,1}$  represent hopping, Rashba spin-orbit coupling, altermagnet strength, and superconducting pairing amplitudes, and we have included the parameters  $0 < b_{1,2,3} < 1$  to represent anisotropic distortions along the  $y$  direction for hopping, magnetic, and superconducting strength, respectively. The parameters  $b_{1,2}$  are generically independent; for example, hopping anisotropy where  $b_1 \neq 1$  need not change the magnetic structure [39]. Since we find  $b_2 \neq 1$  does not qualitatively change the results, we set  $b_2 = 1, t = 1$  in the following. Interestingly, in the absence of superconductivity, an altermagnet can be gapped out and turn into a Chern insulator by applying a weak uniform magnetization. However, because our focus is on TSCs with zero net magnetization we do not consider any uniform external magnetization. We now discuss three important limits (I–III) of Eq. (2).

(I) *Altermagnet- $s$ -wave SC*: First consider isotropic  $s$ -wave pairing,  $\Delta_0 \neq 0, \Delta_1 = 0$ . Figure 3(a) shows the  $x$ -normal boundary spectra of Eq. (2) for  $J_A \neq 0$ , with  $b_1 = 1$ . For  $J_A = 0$  the normal state has two Rashba-like Fermi surfaces around the  $\Gamma$  point, yielding a fully gapped trivial superconducting phase (see Appendix D [29]). In contrast, for  $J_A = 0.3$ , the normal state has one Fermi surface around  $\Gamma$  and another around  $M$ , yielding a weak TSC with vanishing Chern number, but hosting two Majorana edge modes of opposite chirality protected by translation symmetry, e.g., on an  $x$ -normal edge there is one mode each at  $k_y = 0, \pi$ . Adding a slight crystal anisotropy, e.g.,  $b_1 = 0.85$ , a strong chiral TSC with SC Chern number  $|\mathcal{N}| = 1$  appears despite the vanishing net magnetization [see Fig. 3(b)]. The anisotropy of the altermagnet forces the CMFs to reside at different momenta for edges related by a  $\pi/2$  rotation, e.g., we find a chiral mode at  $k_y = 0$  on an  $x$ -normal edge, but at  $k_x = \pi$  for a  $y$ -normal edge. This configuration is reversed by changing the sign of  $\mu$  (relative to half-filling); hence a momentum-resolved spectroscopy measurement would observe alternating profiles between  $x$ - and  $y$ -normal edges as a function of doping or gating. Similar to the 1D case, the topological phase depends on the orientation of the altermagnet. We show in Appendix E [29] that a  $d_{xy}$ -wave altermagnet yields a topologically trivial phase, illustrating again the role of crystal anisotropy as a tuning knob for topological superconductivity.

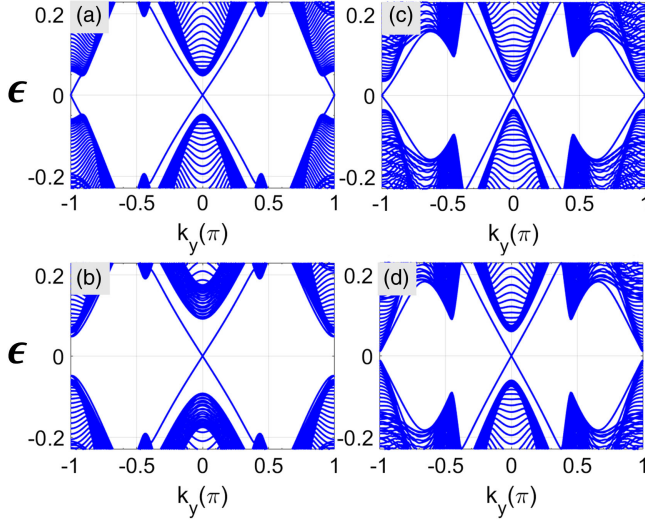


FIG. 3. The  $x$ -normal edge spectrum of the altermagnet-SC heterojunction in Eq. (2) with  $s$  (a),(b) and  $s_{\pm}$ -wave (c),(d) pairings. (a)  $\Delta_0 = 0.3$ ,  $b_1 = 1$ ,  $J_A = 0.3$ , (b)  $\Delta_0 = 0.3$ ,  $b_1 = 0.85$ ,  $J_A = 0.3$ , (c)  $\Delta_0 = 0.4$ ,  $\Delta_1 = 0.3$ ,  $b_1 = 1$ ,  $b_3 = 1$ ,  $J_A = 0.3$ , (d)  $\Delta_0 = 0.4$ ,  $\Delta_1 = 0.3$ ,  $b_1 = 1$ ,  $b_3 = 0.8$ ,  $J_A = 0.3$ . For all plots,  $\mu = -0.4$ ,  $\lambda_R = 0.3$ ,  $t = 1$ .

(II) Altermagnet-anisotropic  $s + s_{\pm}$ -wave SC: Similar topological phases for an isotropic crystal are obtained by resorting to a slightly anisotropic  $s_{\pm}$  pairing, i.e.,  $\Delta_0, \Delta_1 \neq 0, 0 < b_3 < 1$ . Figure 3(c) shows the  $x$ -normal boundary spectra with  $J_A \neq 0$  and  $b_3 = 1$ . Similar to limit (I), a weak TSC is generated with isotropic  $s_{\pm}$  and nonvanishing altermagnetism [see Fig. 3(c)] while the case with vanishing altermagnetism is trivial (see Appendix E [29]). Including a small anisotropy in the pairing,  $b_3 \neq 1$ , yields a chiral TSC with  $|\mathcal{N}| = 1$ , Fig. 3(d). In contrast to (I), the momenta of the Majorana modes on each edge are correlated to the sign (phase) difference between  $\Delta_0$  and  $\Delta_1$  instead of the sign of  $\mu$ .

(III) Altermagnet- $s + d$ -wave SC: Adding a small real  $d$ -wave pairing component (see Appendix F [29] for  $s + id$  pairing) to limit (I) yields a fully gapped chiral TSC with  $\mathcal{N} \neq 0$  without the need for crystal anisotropy. Indeed, Fig. 4(a) shows that the edge spectrum for  $\Delta_0 = 2\Delta_1$  and  $b_1 = 1, b_3 = -1$  hosts CMFs such that  $|\mathcal{N}| = 1$ . While this Letter has focused on fully gapped TSCs, increasing the strength of  $\Delta_1 > \Delta_0$  creates bulk nodes in the superconducting state; the CMFs can survive as shown in Fig. 4(b).

*Majorana corner modes: SC/2D TI/Altermagnet heterostructures*—As a final application, we demonstrate routes to higher order topology using altermagnets. We show Majorana corner modes in a heterostructure where a  $d$ -wave altermagnet is adjacent to a SC-proximitized 2D TI, depicted in Fig. 1(c) [40]. In Appendix G [29], we show that a  $g$ -wave altermagnet also yields Majorana corner modes, but with different phenomenology.

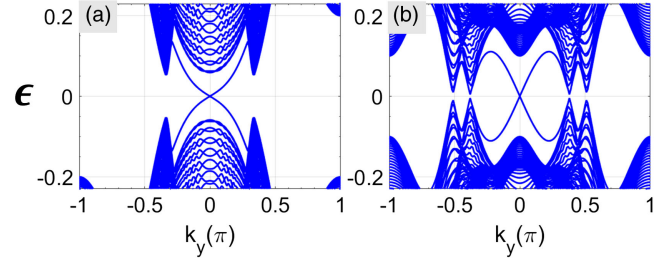


FIG. 4. The  $x$ -normal edge spectrum of the altermagnet-SC heterojunction in Eq. (2) with  $s + d$ -wave pairing. (a)  $\Delta_0 = 0.4$ ,  $\Delta_1 = 0.2$ ,  $\mu = 0$ ,  $b_1 = 1$ ,  $J_A = 0.3$ , (b)  $\Delta_0 = 0.1$ ,  $\Delta_1 = 0.3$ ,  $\mu = 0$ ,  $b_1 = 1$ ,  $J_A = 0.3$ .  $t = 1$ ,  $b_3 = -1$ , and  $\lambda_R = 0.3$  is used for all plots.

Consider the following Hamiltonian for a normal-state 2D time-reversal invariant TI coupled to a  $d_{x^2-y^2}$ -wave altermagnet:

$$h_{TI}(\mathbf{k}) = A(\mathbf{k}) + M(\mathbf{k}) + J_A(\mathbf{k}), \quad (3)$$

where  $A(\mathbf{k}) = A[\sin(k_x)\kappa^z\sigma^x + \sin(k_y)\kappa^z\sigma^y]$ ,  $M(\mathbf{k}) = [B + t(4 - 2[\cos(k_x) + \cos(k_y)])]\kappa^x$ ,  $J_A(\mathbf{k}) = J_A[\cos(k_x) - \cos(k_y)]\kappa^z\sigma^z$  and  $\kappa^i$  and  $\sigma^i$  are Pauli matrices that denote orbital and spin spaces. In the limit  $J_A = 0$  and  $0 < -B < 8t$ , Eq. (3) describes a 2DTI exhibiting helical edges states. Upon proximitizing with an altermagnet, i.e., turning on  $J_A \neq 0$ , Eq. (3) becomes a HOTI protected by  $C_4T$  symmetry that hosts single, complex fermion corner modes and fractional  $e/2$  corner charges. Such a Hamiltonian is experimentally feasible: the 2D TI layer could be, e.g., HgTe, WTe<sub>2</sub>, bismuthene on SiC or a monolayer iron chalcogenide [43–45], and the altermagnet could be one of the materials described in Ref. [20] such as RuO<sub>2</sub>.

We now consider adding superconductivity. There are six possible antisymmetric,  $k$ -independent superconducting pairing terms,  $\Delta^i, i = 0, \dots, 6$ . We leave a discussion of each of the pairing terms to future work, and here focus only on two options. First, upon proximitizing the HOTI phase with the simplest intraorbital spin singlet pairing of the form  $\Delta^1 = \kappa^0\sigma^2$ , the complex fermion corner states become a pair of MZMs and gap out. However, as we found in 1D, when the chemical potential  $\mu$  is tuned to zero, there is a regime where the pair of MZMs corner modes survive. Since the superconductivity competes with the altermagnetism, we expect that as the pairing increases the edges will undergo a transition between a phase gapped by altermagnetism and a phase gapped by superconductivity, the latter of which has no corner modes. To illustrate, at a fixed pairing strength, Fig. 5(a) shows that a critical strength of the altermagnetism is required to generate the pair of Majorana corner modes when  $\mu = 0$ . The transition from trivial to higher order superconducting phases occurs

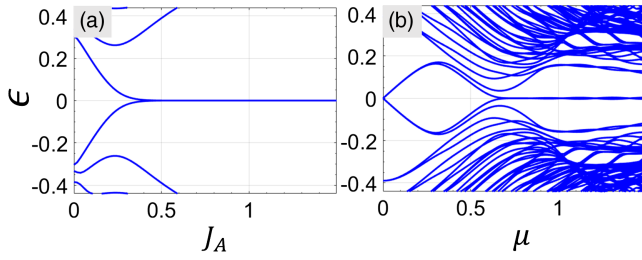


FIG. 5. The corner spectrum of a 2D TI proximitized by altermagnetism and a SC with pairing (a)  $\Delta^1$  versus  $J_A$  for  $\mu = 0$  or pairing (b)  $\Delta^4$  versus  $\mu$  for  $J_A = 0.5$ .  $A = 1$ ,  $B = -0.8$ ,  $t = 0.5$ ,  $\Delta = 0.3$  is used for both plots.

at the edges of the sample, providing a superconducting analog of a boundary obstructed topological phase [46].

Second, consider a spin-triplet pairing  $\Delta^4 = \kappa^2 \sigma^1$ . Momentarily ignoring the altermagnetism, this model describes a time-reversal-invariant first-order TSC in class DIII when the chemical potential enters the bulk bands. Such a system harbors helical Majorana edge states that will immediately be gapped by altermagnetism in a spatially alternating pattern, leading to corner MZMs as shown in Fig. 5(b).

*Discussion*—We remark on the experimental outlook. Altermagnets vastly expand the possible material platforms to realize Majorana fermions. Already, 60 materials are proposed to exhibit altermagnetic order [47].  $\text{RuO}_2$ ,  $\text{Mn}_5\text{Si}_3$ ,  $\text{MnF}_2$ , and  $\text{MnO}_2$  are among most studied  $d$ -wave altermagnets, while  $\text{CrSb}$  and  $\text{MnTe}$  are among  $g$ -wave ones. Furthermore, altermagnetism may be induced in conventional 2D antiferromagnets by an external electric field [48]. Our Letter will catalyze first-principles calculations on these materials to find the most suitable candidates.

In addition, altermagnets with sizable SOC (while maintaining  $\lambda \ll J_A$ ) allow for simpler platforms that do not require a semiconductor (in one dimension) or a 3D TI surface (in two dimensions). Follow-up work will study multiband effects from quantum confinement in 1D altermagnetic wires. Recently, we showed that the 2D effective Hamiltonian in Eq. (2) is a good description of both a 2D altermagnet or a thin film of a 3D altermagnet [49].

Furthermore, the anisotropic nature of magnetic order in altermagnets warrants further study on which interfaces or facets show the strongest altermagnetic order. Recently, a first-principles study of an altermagnet on a TI demonstrated that only specific surfaces of the TI are amenable to induced altermagnetic order [50]. This study demonstrates the experimental feasibility of our proposal, as well as the importance of detailed follow-up on specific surfaces.

In conclusion, Majorana heterostructures made from altermagnets offer several advantages over those with uniform order by providing new tuning knobs and vanishing net magnetization in a wealth of new materials. The 1D and 2D setups we proposed will further generalize to 3D

topological phases [51–54]. Thus, our Letter provides a launching point for many future studies of both new materials and new platforms in the quest to realize Majorana fermions.

*Acknowledgments*—This work was supported by the Air Force Office of Scientific Research under Grant No. FA9550-20-1-0260. J.C. is partially supported by the Alfred P. Sloan Foundation through a Sloan Research Fellowship. The Flatiron Institute is a division of the Simons Foundation. T.L.H. was supported by the Center for Quantum Sensing and Quantum Materials, an Energy Frontier Research Center funded by the U.S. Department of Energy, Office of Science, Basic Energy Sciences under Award No. DE-SC0021238. This research is completed during the program “A Quantum Universe in a Crystal: Symmetry and Topology across the Correlation Spectrum” at the Kavli Institute for Theoretical Physics, supported in part by the National Science Foundation under Grant No. NSF PHY-1748958.

- [1] M. Sato and Y. Ando, Topological superconductors: A review, *Rep. Prog. Phys.* **80**, 076501 (2017).
- [2] T. Yukio, S. Masatoshi, and N. Naoto, Symmetry and topology in superconductors, *J. Phys. Soc. Jpn.* **81**, 011013 (2012).
- [3] C.-K. Chiu, J. C. Y. Teo, A. P. Schnyder, and S. Ryu, Classification of topological quantum matter with symmetries, *Rev. Mod. Phys.* **88**, 035005 (2016).
- [4] C. Nayak, S. H. Simon, A. Stern, M. Freedman, and S. Das Sarma, Non-Abelian anyons and topological quantum computation, *Rev. Mod. Phys.* **80**, 1083 (2008).
- [5] R. M. Lutchyn, J. D. Sau, and S. Das Sarma, Majorana fermions and a topological phase transition in semiconductor-superconductor heterostructures, *Phys. Rev. Lett.* **105**, 077001 (2010).
- [6] S. Nadj-Perge, I. K. Drozdov, B. A. Bernevig, and A. Yazdani, Proposal for realizing Majorana fermions in chains of magnetic atoms on a superconductor, *Phys. Rev. B* **88**, 020407(R) (2013).
- [7] M. Hell, M. Leijnse, and K. Flensberg, Two-dimensional platform for networks of Majorana bound states, *Phys. Rev. Lett.* **118**, 107701 (2017).
- [8] F. Pientka, A. Keselman, E. Berg, A. Yacoby, A. Stern, and B. I. Halperin, Topological superconductivity in a planar Josephson junction, *Phys. Rev. X* **7**, 021032 (2017).
- [9] M. Luethi, H. F. Legg, K. Laubscher, D. Loss, and J. Klinovaja, Majorana bound states in germanium Josephson junctions via phase control, *Phys. Rev. B* **108**, 195406 (2023).
- [10] O. Lesser, Y. Oreg, and A. Stern, One-dimensional topological superconductivity based entirely on phase control, *Phys. Rev. B* **106**, L241405 (2022).
- [11] S. Vaitiekėnas, G. Winkler, B. Van Heck, T. Karzig, M.-T. Deng, K. Flensberg, L. Glazman, C. Nayak, P. Krogstrup, R. Lutchyn *et al.*, Flux-induced topological superconductivity in full-shell nanowires, *Science* **367**, eaav3392 (2020).

- [12] S. Nadj-Perge, I. K. Drozdov, J. Li, H. Chen, S. Jeon, J. Seo, A. H. MacDonald, B. A. Bernevig, and A. Yazdani, Observation of Majorana fermions in ferromagnetic atomic chains on a superconductor, *Science* **346**, 602 (2014).
- [13] X.-L. Qi, T. L. Hughes, and S.-C. Zhang, Chiral topological superconductor from the quantum Hall state, *Phys. Rev. B* **82**, 184516 (2010).
- [14] J. Wang, Q. Zhou, B. Lian, and S.-C. Zhang, Chiral topological superconductor and half-integer conductance plateau from quantum anomalous Hall plateau transition, *Phys. Rev. B* **92**, 064520 (2015).
- [15] S. Das Sarma, In search of Majorana, *Nat. Phys.* **19**, 165 (2023).
- [16] H. Pan and S. Das Sarma, Physical mechanisms for zero-bias conductance peaks in Majorana nanowires, *Phys. Rev. Res.* **2**, 013377 (2020).
- [17] M. Kayyalha, D. Xiao, R. Zhang, J. Shin, J. Jiang, F. Wang, Y.-F. Zhao, R. Xiao, L. Zhang, K. M. Fijalkowski *et al.*, Absence of evidence for chiral Majorana modes in quantum anomalous hall-superconductor devices, *Science* **367**, 64 (2020).
- [18] M. Aghaee, A. Akkala, Z. Alam, R. Ali, A. A. Ramirez, M. Andrzejczuk, A. E. Antipov, M. Astafev, B. Bauer, J. Becker *et al.*, InAs-Al hybrid devices passing the topological gap protocol, *Phys. Rev. B* **107**, 245423 (2023).
- [19] L. Šmejkal, J. Sinova, and T. Jungwirth, Beyond conventional ferromagnetism and antiferromagnetism: A phase with nonrelativistic spin and crystal rotation symmetry, *Phys. Rev. X* **12**, 031042 (2022).
- [20] L. Šmejkal, J. Sinova, and T. Jungwirth, Emerging research landscape of altermagnetism, *Phys. Rev. X* **12**, 040501 (2022).
- [21] H. Bai, Y. C. Zhang, Y. J. Zhou, P. Chen, C. H. Wan, L. Han, W. X. Zhu, S. X. Liang, Y. C. Su, X. F. Han, F. Pan, and C. Song, Efficient spin-to-charge conversion via altermagnetic spin splitting effect in antiferromagnet RuO<sub>2</sub>, *Phys. Rev. Lett.* **130**, 216701 (2023).
- [22] I. I. Mazin, Altermagnetism in MnTe: Origin, predicted manifestations, and routes to detwinning, *Phys. Rev. B* **107**, L100418 (2023).
- [23] J. A. Ouassou, A. Brataas, and J. Linder, Josephson effect in altermagnets, *Phys. Rev. Lett.* **131**, 076003 (2023).
- [24] S.-B. Zhang, L.-H. Hu, and T. Neupert, Finite-momentum Cooper pairing in proximitized altermagnets, *Nat. Commun.* **15**, 1801 (2024).
- [25] M. Papaj, Andreev reflection at altermagnet/superconductor interface, *Phys. Rev. B* **108**, L060508 (2023).
- [26] X. Zhou, W. Feng, R.-W. Zhang, L. Šmejkal, J. Sinova, Y. Mokrousov, and Y. Yao, Crystal thermal transport in altermagnetic RuO<sub>2</sub>, *Phys. Rev. Lett.* **132**, 056701 (2024).
- [27] D. Zhu, Z.-Y. Zhuang, Z. Wu, and Z. Yan, Topological superconductivity in two-dimensional altermagnetic metals, *Phys. Rev. B* **108**, 184505 (2023).
- [28] C. Wu, K. Sun, E. Fradkin, and S.-C. Zhang, Fermi liquid instabilities in the spin channel, *Phys. Rev. B* **75**, 115103 (2007).
- [29] See Supplemental Material at <http://link.aps.org/supplemental/10.1103/PhysRevLett.133.106601> for (i) altermagnet-nanowire proximity simulation, (ii) discussion on maximum SC gap in altermagnet vs uniform magnetization setups, (iii) Chiral states in altermagnet/TI platforms, (iv) spectrum for  $s + s_{\pm}$  with  $J_A = 0$ , (v)  $d_{x^2-y^2}$  vs  $d_{xy}$  altermagnet-SC heterostructures, (vi) spectrum for  $s + id$ -wave pairing, (vii) discussion on 2D TI/G-wave/SC.
- [30] S. Tewari and J. D. Sau, Topological invariants for spin-orbit coupled superconductor nanowires, *Phys. Rev. Lett.* **109**, 150408 (2012).
- [31] A. P. Schnyder, S. Ryu, A. Furusaki, and A. W. W. Ludwig, Classification of topological insulators and superconductors in three spatial dimensions, *Phys. Rev. B* **78**, 195125 (2008).
- [32] A. P. Schnyder, S. Ryu, A. Furusaki, and A. W. W. Ludwig, Classification of topological insulators and superconductors, *AIP Conf. Proc.* **1134**, 10 (2009).
- [33] A. Kitaev, Periodic table for topological insulators and superconductors, *AIP Conf. Proc.* **1134**, 22 (2009).
- [34] C.-X. Liu, J. D. Sau, T. D. Stanescu, and S. Das Sarma, Andreev bound states versus Majorana bound states in quantum dot-nanowire-superconductor hybrid structures: Trivial versus topological zero-bias conductance peaks, *Phys. Rev. B* **96**, 075161 (2017).
- [35] W. P. Su, J. R. Schrieffer, and A. J. Heeger, Solitons in polyacetylene, *Phys. Rev. Lett.* **42**, 1698 (1979).
- [36] L. Fu and C. L. Kane, Superconducting proximity effect and Majorana fermions at the surface of a topological insulator, *Phys. Rev. Lett.* **100**, 096407 (2008).
- [37] W. A. Benalcazar, B. A. Bernevig, and T. L. Hughes, Electric multipole moments, topological multipole moment pumping, and chiral hinge states in crystalline insulators, *Phys. Rev. B* **96**, 245115 (2017).
- [38] F. Schindler, A. M. Cook, M. G. Vergniory, Z. Wang, S. S. Parkin, B. A. Bernevig, and T. Neupert, Higher-order topological insulators, *Sci. Adv.* **4**, eaat0346 (2018).
- [39] L. Šmejkal, R. González-Hernández, T. Jungwirth, and J. Sinova, Crystal time-reversal symmetry breaking and spontaneous Hall effect in collinear antiferromagnets, *Sci. Adv.* **6**, eaaz8809 (2020).
- [40] The setup is similar to that proposed in Refs. [41,42], but with the uniform magnetic field substituted by altermagnetic order.
- [41] Y.-J. Wu, J. Hou, Y.-M. Li, X.-W. Luo, X. Shi, and C. Zhang, In-plane Zeeman-field-induced Majorana corner and hinge modes in an  $s$ -wave superconductor heterostructure, *Phys. Rev. Lett.* **124**, 227001 (2020).
- [42] Z. Yan, Majorana corner and hinge modes in second-order topological insulator/superconductor heterostructures, *Phys. Rev. B* **100**, 205406 (2019).
- [43] B. A. Bernevig, T. L. Hughes, and S.-C. Zhang, Quantum spin Hall effect and topological phase transition in HGTE quantum wells, *Science* **314**, 1757 (2006).
- [44] X. Qian, J. Liu, L. Fu, and J. Li, Quantum spin Hall effect in two-dimensional transition metal dichalcogenides, *Science* **346**, 1344 (2014).
- [45] F. Reis, G. Li, L. Dudy, M. Bauernfeind, S. Glass, W. Hanke, R. Thomale, J. Schäfer, and R. Claessen, Bismuthene on a SiC substrate: A candidate for a high-temperature quantum spin Hall material, *Science* **357**, 287 (2017).
- [46] E. Khalaf, W. A. Benalcazar, T. L. Hughes, and R. Queiroz, Boundary-obstructed topological phases, *Phys. Rev. Res.* **3**, 013239 (2021).

- [47] Y. Guo, H. Liu, O. Janson, I. C. Fulga, J. van den Brink, and J. I. Facio, Spin-split collinear antiferromagnets: A large-scale ab-initio study, *Mater. Today Phys.* **32**, 100991 (2023).
- [48] I. Mazin, R. González-Hernández, and L. Šmejkal, Induced monolayer altermagnetism in  $\text{MnP}(\text{S, Se})_3$  and FeSe, [arXiv: 2309.02355](https://arxiv.org/abs/2309.02355).
- [49] Y. Fang, J. Cano, and S. A. A. Ghorashi, Quantum geometry induced nonlinear transport in altermagnets, *Phys. Rev. Lett.* **133**, 106701 (2024).
- [50] R. M. Sattigeri, G. Cuono, and C. Autieri, Altermagnetic surface states: Towards the observation and utilization of altermagnetism in thin films, interfaces and topological materials, *Nanoscale* **15**, 16998 (2023).
- [51] S. A. A. Ghorashi, J. Cano, E. Rossi, and T. L. Hughes, Higher-order nodal hinge states in doped superconducting topological insulator, *Phys. Rev. B* **108**, 094504 (2023).
- [52] S. A. A. Ghorashi, T. L. Hughes, and E. Rossi, Vortex and surface phase transitions in superconducting higher-order topological insulators, *Phys. Rev. Lett.* **125**, 037001 (2020).
- [53] S. A. A. Ghorashi, T. Li, and T. L. Hughes, Higher-order Weyl semimetals, *Phys. Rev. Lett.* **125**, 266804 (2020).
- [54] S. A. A. Ghorashi, X. Hu, T. L. Hughes, and E. Rossi, Second-order Dirac superconductors and magnetic field induced Majorana hinge modes, *Phys. Rev. B* **100**, 020509(R) (2019).